Oxidation of copper electrodes on flexible polyimide substrates for non-enzymatic glucose sensing

View the article online for updates and enhancements.

Materials Research Express

PAPER

Oxidation of copper electrodes on flexible polyimide substrates for non-enzymatic glucose sensing

Shijia Liu[1,4], Ayse Ay[1,4], Qiaochu Luo[1,5], Xiangqi Hu[1], Katarzyna Białas[2], Gorachand Dutta[2,6], Despina Moschou[2] and Anna Regoutz[3]

1   Department of Materials, Imperial College London, South Kensington, London SW7 2AZ, United Kingdom
2   Centre for Biosensors, Bioelectronics and Biodevices (C3Bio) and Department of Electronic and Electrical Engineering, University of Bath, Bath, BA2 7AY, United Kingdom
3   Department of Chemistry, University College London, 20 Gordon Street, London, WC1H 0AJ, United Kingdom
4   Both authors contributed equally to the manuscript.
5   Present address: Faculty of Natural Sciences and Engineering, Sabanci University, Tuzla, Istanbul 34956, Turkey.
6   Present address: School of Medical Science and Technology (SMST), Indian Institute of Technology Kharagpur, Kharagpur, West Bengal 721302, India.

E-mail: a.regoutz@ucl.ac.uk

Supplementary material for this article is available online

Abstract

The integration of non-enzymatic glucose sensing entities into device designs compatible with industrial production is crucial for the broad take-up of non-invasive glucose sensors. Copper and its oxides have proven to be promising candidates for electrochemical glucose sensing. They can be fabricated *in situ* enabling integration with standard copper metallisation schemes for example in printed circuit boards (PCBs). Here, copper oxide electrodes are prepared on flexible polyimide substrates through direct annealing of patterned electrode structures. Both annealing temperature and duration are tuned to optimise the sensor surface for optimum glucose detection. A combination of microscopy and spectroscopy techniques is used to follow changes to the surface morphology and chemistry under the varying annealing conditions. The observed physico-chemical electrode characteristics are directly compared with electrochemical testing of the sensing performance, including chronoamperommetry and interference experiments. A clear influence of both aspects on the sensing behaviour is observed and an anneal at 250 °C for 8 h is identified as the best compromise between sensor performance and low interference from competing analytes.

1. Introduction

Diabetes is a chronic and metabolic disease in which the pancreas cannot produce enough insulin or in which the body becomes resistant to insulin. It is one of the main causes of kidney failure, vision loss, and cardiac and nervous system diseases, and it can affect every organ of the human body. The Diabetes Atlas of the International Diabetes Federation (IDF) reports that there are 537 million people living with diabetes in 2021 and by 2045 this number is predicted to rise to 784 million people [1]. There is no cure for diabetes available, and hence controlling blood sugar levels through diet, exercise, and drugs is essential. Continuous blood sugar monitoring is necessary to improve the quality of life of diabetes patients, with usual blood sugar levels in the 220 mM range. The majority of sensors to date are based on enzymatic sensing approaches, which have superior selectivity, but suffer from stability and related storage limitations [2, 3]. To overcome these limitations, non-enzymatic alternatives are being developed, which rely on the direct oxidation of glucose [4, 5]. A range of inorganic materials, which catalyse the electrochemical oxidation, have been explored with transition metal oxides dominating the field, including Mn, Co, Ni, Cu, Zn and Ru [5–7]. The reasons for the widespread use of metal oxides in glucose sensing include their low cost, stability, high synthesis control, and favourable electron transfer properties.

In addition to changing the sensing entity, a parallel avenue of development is the search for alternatives to the traditional prick tests used to extract blood. A wide range of non-invasive glucose biosensors are being developed [8–11]. Many non-invasive test designs rely not on the measurement of blood glucose levels, but on glucose detection in other fluids, such as interstitial fluid, saliva, sweat or urine. This presents an additional challenge for glucose sensors as glucose concentrations found in these fluids are much lower compared to blood and therefore require lower detection limits [10, 12].

A particularly popular candidate family for non-enzymatic glucose sensors, that can address many of the demands for non-invasive designs, are copper and its oxides. They offer low cost, low toxicity, accessible synthesis routes, good optical and electrical characteristics, and the ability to tune their morphology and structure [1, 13–20]. A number of review articles has covered recent advances across different aspects of copper oxide nanoparticles for glucose sensing in detail [21–25]. Two main synthesis strategies exist that can be used to prepare copper oxide sensors. Either nanostructures are synthesised *ex situ* and then applied to a conductive substrate, e.g. through drop casting or printing, or they can be synthesised directly, *in situ*, on the surface of a conducting electrode, e.g. Cu or C [26–29]. The advantage of the *ex situ* approach is a higher level of control of resulting particle sizes and morphology, but *in situ* approaches promise an organic incorporation in existing large scale device production. Polymer-based printed circuit boards (PCBs) are one widely used design platform in Lab-on-Chip biosensing microsystem technology as they offer low cost and consistent manufacturing of electronics-integrated biodevices. Low cost solutions are of increasing importance as over 4 in 5 (81%) adults with diabetes live in low- and middle-income countries [1]. In this respect, the incorporation of the inorganic sensing entities into existing substrate technologies is of great importance, promising a unique biosensor alternative for increased stability and shelf-life of functionalised sensing electrodes, over enzyme-based modifications. Flexible, polyimide-based Lab-on-PCB microsystems are of particular importance for wearable applications, with glucose quantification one of the major areas of interest [30].

One of the major challenges in building up a fundamental understanding, and to ultimately design more improved biosensors, of any nanostructure used in glucose sensing is that nanostructures significantly differ from their micron-scale or extended bulk counterparts. Whilst binary bulk metal oxides are in general well understood, any findings from bulk theory or experiment cannot be easily extrapolated to nanostructures. Across the majority of the existing literature, the only physical characterisation routinely used to correlate sensing properties with is the surface morphology probed by microscopy techniques. Whilst surface morphology plays an important role in the sensing characteristics of a material, it is not the only influencing parameter. Surface chemistry, which is not widely explored in non-enzymatic glucose sensors, will play a major role and the initial distribution of Cu oxidation states present at the sensor surface, from metallic Cu, to Cu in its +1 and +2 oxidation states, is crucial.

This work reports the successful formation of nanostructured copper oxide electrodes on a flexible, polyimide substrate. The influence of both annealing temperature and duration is explored systematically to define the optimum manufacturing parameters for best sensing performance. In order to provide a comprehensive discussion of the influence of both surface morphology and chemistry, imaging techniques, including atomic force microscopy (AFM) and scanning electron microscopy (SEM), are combined with x-ray photoelectron spectroscopy (XPS). The results from the physical and chemical characterisation of the electrode surfaces are then directly related to their electrochemical sensing performance, including cyclic voltammetry and chronoamperometry.

2. Experimental methods

Copper electrode structures were prepared on flexible polyimide substrates as follows. A dry negative photoresist (Fortex, UK) was applied at 110 °C on copper-clad polyimide films, and exposed by UV light (wavelength: 360–380 nm, energy: 30–35 mJ cm^{-2}) through a metal mask for 2 min. Following that, the samples were post baked for 1 min at 120 °C and kept at room temperature in the developer solution for 2 min. A ferric chloride solution was used as a copper etchant to remove the copper layer from the polyimide film, and samples were dipped in acetone to remove the negative polyimide photoresist. To achieve oxidation of the copper electrodes and formation of copper oxide overlayers, the copper electrodes on polyimide films were annealed at varying times and temperatures. Temperatures from 100 °C–400 °C at a constant annealing duration of 5 h and annealing duration of 1–24 h at a constant temperature of 250 °C were explored. Electrodes were places in alumina boats and annealed at atmospheric pressure in air in a tube furnace. The heating rate was set at 300 °C/h and no active cooling was used.

The surface morphology and chemistry of the resulting Cu/Cu oxide electrodes was characterised using AFM, SEM, and XPS. AFM characterisation of thermally annealed electrodes was performed on a Nanosurf NaioAFM instrument equipped with a Nanosurf Isostage isolation table. Tapping mode and silicon carbide tips

with reflective aluminium coating (Tap190Al-G, BudgetSensors, resonant frequency 190 kHz, force constant 48 N/m) were used for all samples. Samples were characterised as is without further modification and five measurements were taken for each sample. Raw images were processed using the Gwyddion software package. SEM characterisation was performed on a Jeol-JSM6010PLUS/LA instrument at a voltage of 20 kV. Samples were gold coated before data collection (Quorum Q150RS, current of 50 mA, duration of 30 s). Image analysis was undertaken using the open-source processing package ImageJ, and brightness and contrast optimised. XPS was performed on a Thermo Fischer K-alpha+ instrument with an monochromated Al Kα x-ray source (hν = 1486.6 eV) at an x-ray spot size of 400 μm. A flood gun emitting low energy electrons and Ar+ ions was used to prevent sample charging. Thermally annealed electrodes were mounted onto the sample plate using conducting carbon tape. Survey spectra were collected at a pass energy of 200 eV, while core level spectra used a pass energy of 20 eV. Peak-fitting and data extraction was performed using the Thermo Avantage software package. All core levels are normalised to the height of the Cu $2p_{3/2}$ peak and aligned to the adventitious carbon peak at 284.8 eV (see figure 3 in the supplementary information available online at stacks.iop.org/MRX/9/045010/mmedia for the C $1s$ spectra of all electrodes).
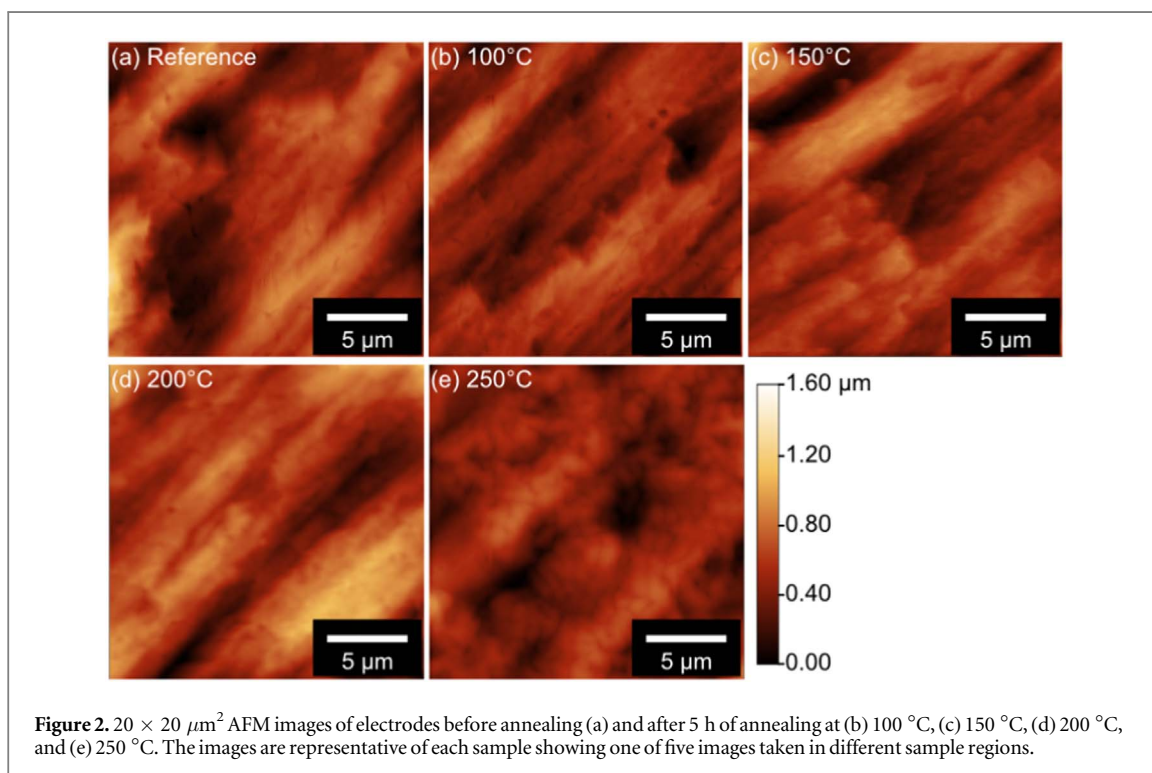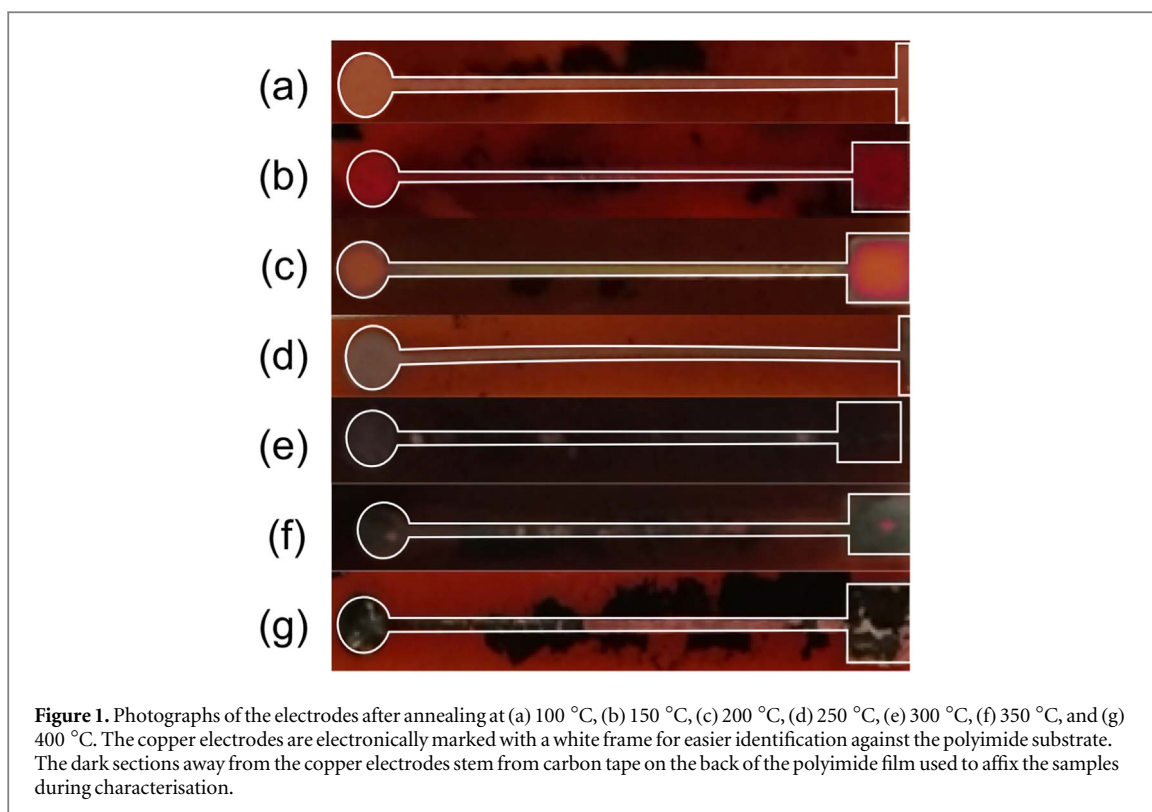
Voltammetric and chronoamperometric tests were conducted on all annealed Cu electrodes. The electrodes were used as working electrodes. Pt wire was used as a counter electrode, and a Ag/AgCl electrode was used as the reference and connected to a potentiostat (Autolab, Netherlands). All electrodes were dipped in 2 mL of glucose solution at different concentrations (1 μM–100 mM) and cyclic voltammetric/chronoamperometric measurements were performed using an electrochemical workstation (Autolab, Netherlands). To ensure the mutarotation of α-D-glucose to β-D-glucose, a 100 mM glucose solution was prepared in 0.1 M NaOH, stored overnight at room temperature, and diluted gradually to 1 μM to test different glucose concentrations. The effect of 0.1 mM solutions of different interfering species, including fructose, galactose, uric acid, and ascorbic acid, was compared to 0.1 mM glucose solutions in 0.1 M NaOH. Sensor readings were taken after 10 s for all calibration curve calculations. All electrochemical data were obtained at 25 °C.

3. Results and discussion

3.1. Surface morphology

To enable the future use of Cu/Cu oxide electrodes in integrated wearable sensor devices, it is important to understand the production limits on flexible substrates, such as the polyimide chosen in this study. To explore this and the temperature-dependent formation of the nanostructures, the first series of annealing tests included annealing electrodes for a constant time of 5 hours at 100 °C, 150 °C, 200 °C, 250 °C, 300 °C, 350 °C, and 400 °C. Higher annealing temperatures are not feasible as the glass transition of the polyimide film (DuPont Kapton HN) is between 360 and 410 °C, and its application temperature range is limited to −269 to 400 °C [31]. The thermally annealed electrodes display a transition from orange/purple colouration (150 °C), to grey (250 °C), and finally to black (300 °C). This is illustrated in figure 1. The observed colour change is indicative of the growth of a Cu_2O layer, which is red, followed by further growth of a layer of CuO, which is grey or black. The oxide layers produced at temperatures higher than 250 °C were found to be very fragile and peeled easily. This is illustrated by figure 1(g), where the black oxide layer on the electrode annealed at 400 °C has partially peeled off, revealing a pink layer of Cu/Cu_2O underneath. The fragility of the oxide layer is due to lattice strain caused by the mismatched lattice parameters of Cu_2O and CuO, a phenomenon that is well-documented in the literature [32]. Due to the fragility of the oxide layer beyond annealing temperatures of 300 °C, these could not be used for sensing tests, as they could not withstand the forces in the electrochemical testing setup. Based on the observations made in the first round of annealing tests, 250 °C was identified as the maximum temperature at which the copper oxide film is stable and delamination does not occur. A second series of annealing tests therefore used a constant annealing temperature of 250 °C at varying annealing times of 1, 2, 3, 5, 8, 12, and 24 h. The duration of thermal oxidation also changed the appearance of the electrodes visibly with the surface getting darker with increasing annealing time, indicating advancing surface oxidation. Peeling of the copper oxide overlayers was observed at longer annealing duration of 8, 12, and 24 h.

The surface morphology of the oxidised copper electrodes was investigated using AFM. Due to peeling of the oxide layer, tapping mode AFM could only be performed on samples annealed at temperatures up to 250 °C. Large, columnar features can be seen across all samples representing the initial morphology of the Cu electrodes (see figure 2). At 250 °C, smaller structures superimposed on the underlying columnar structure are observed, which are attributed to copper oxide layer growth. All samples annealed for varying times at 250 °C present the same morphology (see images in figure 1 in the supplementary information). Root mean square (RMS) roughness values were extracted from AFM measurements of all samples on five locations across each electrode and errors were obtained by calculating the standard deviation of the results (see figure 3). With increasing annealing temperature, the overall roughness decreases by about 40% due to the oxide overlayer formation,

Figure 1. Photographs of the electrodes after annealing at (a) 100 °C, (b) 150 °C, (c) 200 °C, (d) 250 °C, (e) 300 °C, (f) 350 °C, and (g) 400 °C. The copper electrodes are electronically marked with a white frame for easier identification against the polyimide substrate. The dark sections away from the copper electrodes stem from carbon tape on the back of the polyimide film used to affix the samples during characterisation.

Figure 2. $20 \times 20\ \mu m^2$ AFM images of electrodes before annealing (a) and after 5 h of annealing at (b) 100 °C, (c) 150 °C, (d) 200 °C, and (e) 250 °C. The images are representative of each sample showing one of five images taken in different sample regions.

which covers and levels the underlying copper electrode structure. Comparatively, the variations in surface roughness with increasing annealing time are much smaller.

SEM images (see figures 4 and 5) confirm and further expand the observations made using AFM. For electrodes annealed at 100 °C the surface is rough, and features of the Cu electrode, including grain boundaries, can be clearly identified in figure 4(a). For the electrode annealed at 250 °C the onset of clear surface oxide layer growth is observed. Further oxidation at 300 °C results in small features that resemble the beginnings of nanowire growth. Images of the electrode cross section, an example is presented in figure 4(d), highlight the weak interface adhesion between the Cu_2O layer formed directly on the Cu electrode surface and the CuO
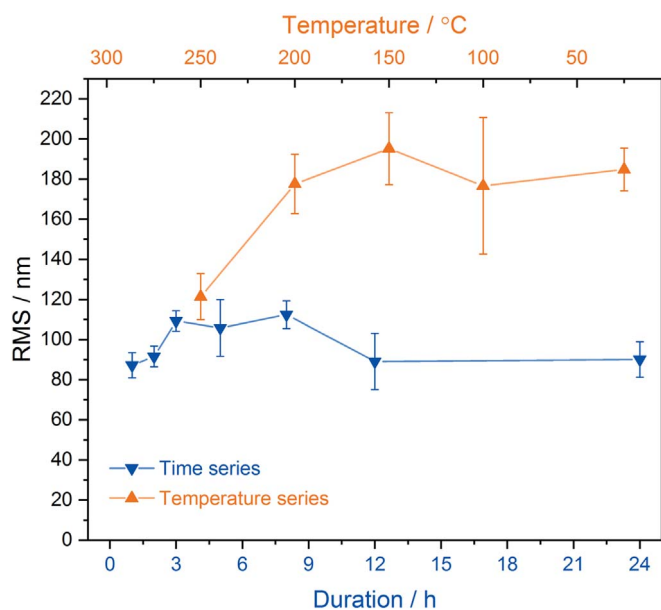
Figure 3. RMS roughness extracted from five $20 \times 20\ \mu m^2$ AFM images for each electrode after annealing at varying temperature and duration.
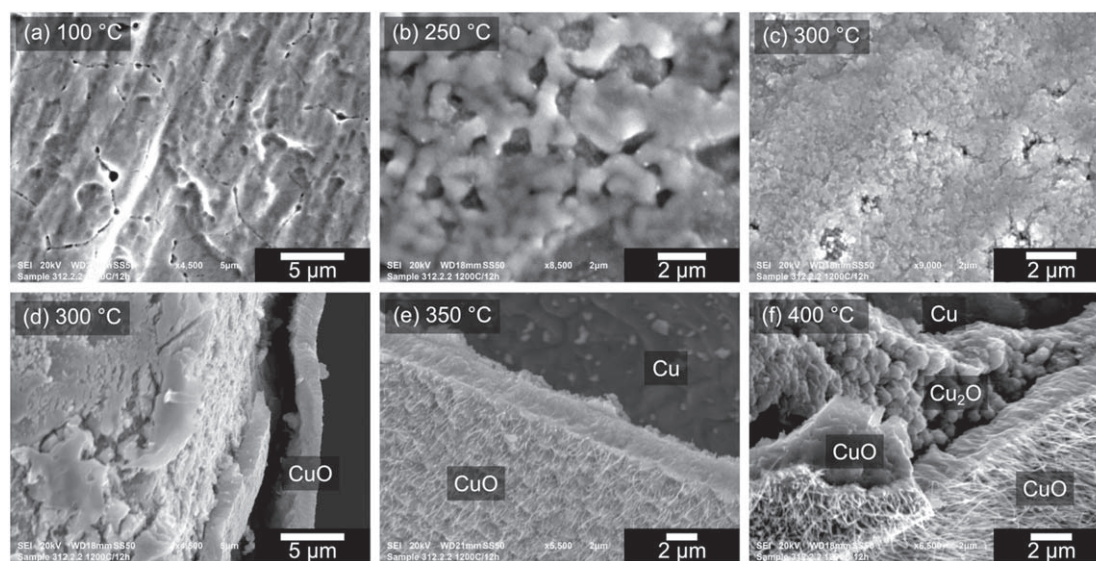

Figure 4. SEM images of electrodes after 5 h of annealing at (a) 100 °C, (b) 250 °C, (c) 300 °C, (d) 300 °C cross section, (e) 350 °C, and (f) 400 °C.

overlayer. Oxidation at 350 °C and 400 °C results in nanowire growth on the electrode surface, with the higher temperature resulting in an increase in nanowire density, in agreement with previous literature reports [17]. After the 400 °C anneal the three layers (Cu metal, Cu_2O, CuO) are well-defined (see figure 4(f)). The Cu_2O layer consists of many faceted grains of 0.5 μm in size, while the CuO nanowires grow from a layer of CuO. The temperature at which nanowire growth is observed in the present study is comparatively higher than previously reported in the literature [4]. This may be due to the existing native oxide layer after the initial electrode fabrication, which can hinder diffusion pathways and suppress initial nanowire growth. More subtle changes to the surface morphology are observed upon increasing the annealing duration at 250 °C. Figure 5 shows representative images of the samples annealed at 3 and 8 h. After 3 h net-like growth of a Cu oxide overlayer is observed, whilst after 8 h a more continuous oxide layer forms

The behaviour upon annealing observed from AFM and SEM is in good agreement with the expected oxidation behaviour of polycrystalline Cu. Initially, Cu_2O starts to form and with prolonged oxidation, a continuous layer will form on the Cu surface. When the Cu_2O layer reaches a critical thickness, the diffusion of
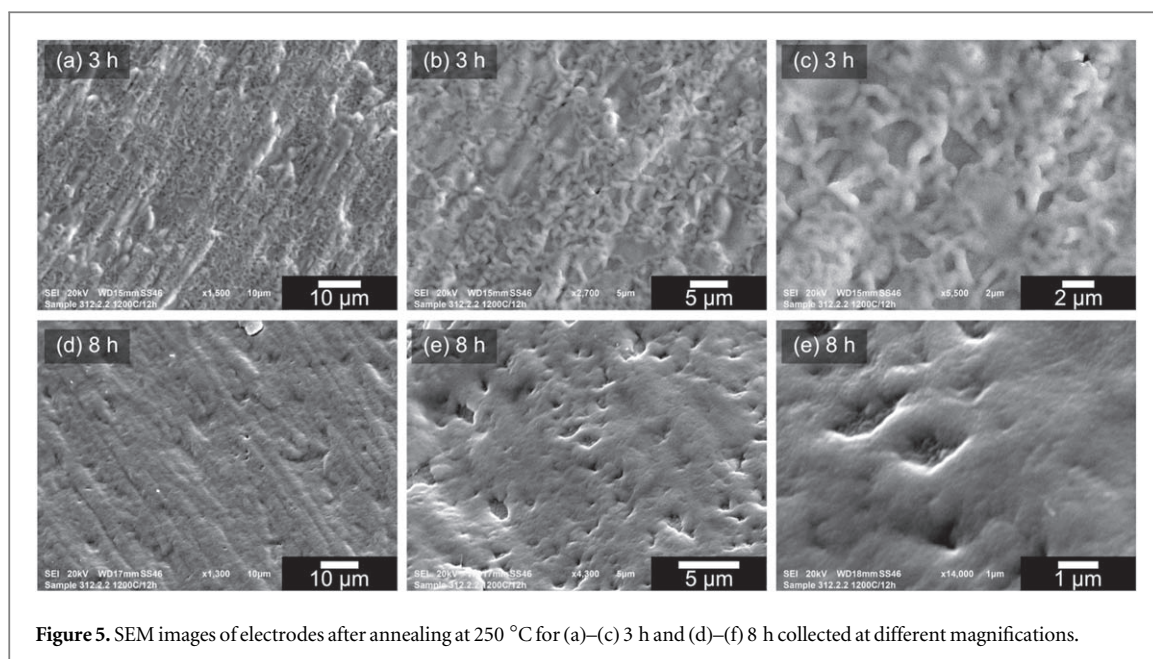
Figure 5. SEM images of electrodes after annealing at 250 °C for (a)–(c) 3 h and (d)–(f) 8 h collected at different magnifications.

oxygen to the underlying Cu substrate is limited and the oxide acts as a passivation layer. Higher temperatures are then necessary to enable further oxidation to CuO, which again with time will form a continuous overlayer. Finally, nanowires begin to grow from the CuO layer. It is clear, that both annealing duration and temperature have a significant influence on the equilibria between the different Cu oxidation states formed on the electrode surfaces.

3.2. Surface chemistry

The ultimate sensing behaviour of these electrodes will depend on both their surface morphology as well as their surface chemistry. In order to investigate the latter, and confirm the inferred chemical states from microscopy, XPS was used. Survey spectra of all samples (see figure 2 in the supplementary information) show the expected core and Auger lines, with minor contributions from C, N, S, Na, and Cl from the initial electrode preparation. In order to investigate the oxidation state and local chemical environments of copper, the Cu $2p_{3/2}$ core level and Cu $L_3M_{4,5}M_{4,5}$ Auger line as well as the O $1s$ core level were collected (see figure 6).

The Cu $2p_{3/2}$ core level for varying annealing temperature and duration are shown in figures 6(a) and (d), respectively. With an increase in annealing temperature a clear shift of the main Cu $2p_{3/2}$ component to higher binding energy (BE) is observed. At temperatures between 100 and 200 °C, the spectra are dominated by the Cu^{+1}/Cu^0 line at 932.5 eV with only a small contribution from Cu^{+2} species visible at higher BE. A CuO component at 933.7 eV and a Cu(OH)$_2$ component at 934.7 eV are observed in varying intensities for all samples. At 250 °C the Cu^{+2} component starts to increase and dominates the spectra of samples annealed at 350 and 400 °C. The spectra collected on samples annealed at varying annealing duration at 250 °C are all dominated by the Cu^{+1}/Cu^0 species at 932.5 eV. With increasing annealing duration an increase of the Cu^{+2} components is observed. The here observed BEs and line shapes of the Cu species agree well with previously reported reference spectra [33–36]. The shift and changes in the main photoionisation line of the Cu $2p_{3/2}$ core level go hand in hand with changes to the satellite features observed between 940 and 945 eV. These satellites are characteristic for Cu^{+2} and originate from shake-up transitions from charge-transfer between ligand O $2p$ and Cu $3d$ states. Such a transfer necessitates a partially filled Cu $3d$ level, as is the case in Cu^{+2} with its $3d^9$ configuration. This can in turn explain the missing of such satellite structures for Cu^{1+}/Cu^0, as the $3d$ level is completely filled ($3d^{10}$) in both. The structure of the observed satellites stems from the multiplet splitting of the $2p^5 3d^9$ final state. More detailed discussions of the satellites can be found in the literature [35, 37–39].

The Cu $2p_{3/2}$ core level cannot be used to distinguish between metallic Cu and Cu^{+1}, as they only exhibit a minimal, non-resolvable chemical shift. To investigate and distinguish between these two oxidation states, the Cu $L_3M_{4,5}M_{4,5}$ Auger line was used (see figures 6(b) and (e) for varying annealing temperature and duration, respectively). The overall Auger line shape changes significantly between metallic Cu and oxidised Cu species, as well as its main feature shifting in BE position [33, 34, 40]. Spectra of samples annealed at temperatures of up to 250 °C are dominated by a line shape and position (570.1 eV) consistent with Cu$_2$O [34, 41]. At higher temperatures the line shifts towards a lower energy of 569.0 eV typical for CuO. As in the Cu $2p_{3/2}$ spectra the Auger line after varying annealing duration at 250 °C is dominated by Cu$_2$O with only a small shoulder from
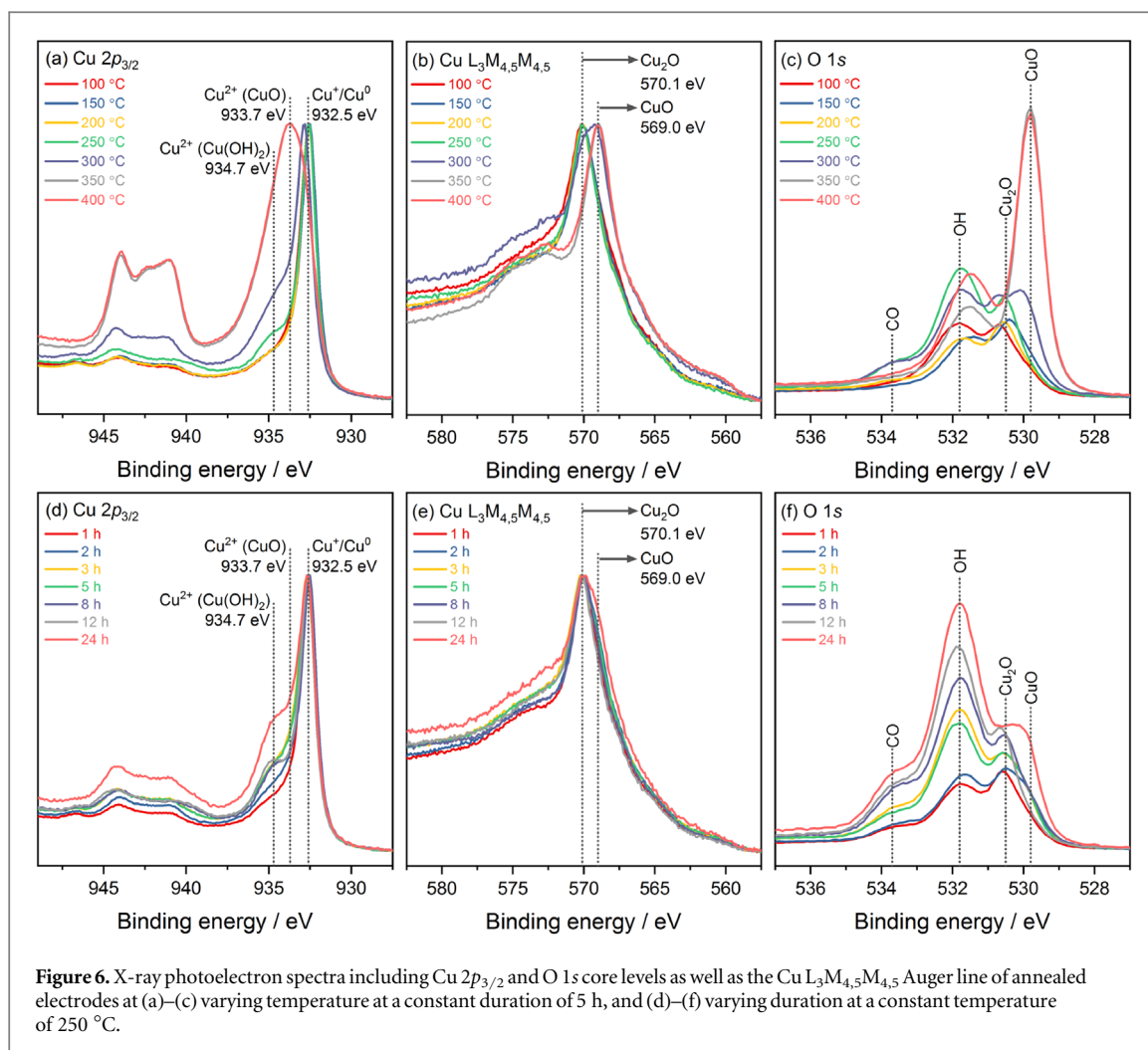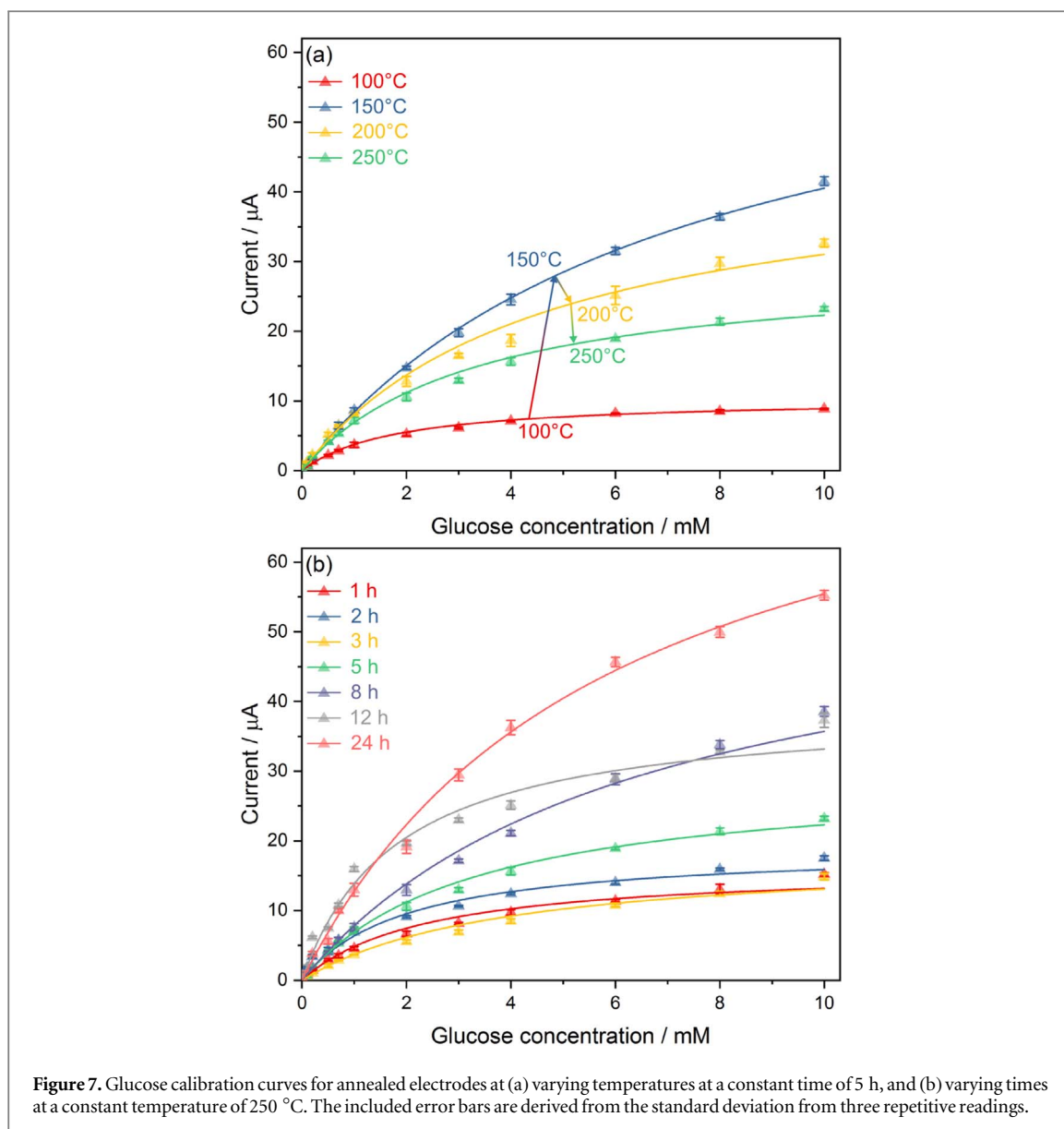
Figure 6. X-ray photoelectron spectra including Cu $2p_{3/2}$ and O $1s$ core levels as well as the Cu $L_3M_{4,5}M_{4,5}$ Auger line of annealed electrodes at (a)–(c) varying temperature at a constant duration of 5 h, and (d)–(f) varying duration at a constant temperature of 250 °C.

CuO discernible. None of the spectra exhibit any features of metallic Cu, which would appear at 568.1 eV [42]. A Wagner plot comparing the Cu $2p_{3/2}$ and Cu $L_3M_{4,5}M_{4,5}$ energies is included in figure 4 in the supplementary information. Based on the observations from the Cu $2p_{3/2}$ core and Cu $L_3M_{4,5}M_{4,5}$ Auger spectra both an increase in annealing temperature as well as annealing duration favours the oxidation of Cu from Cu_2O to CuO. It is clear that except for the highest annealing temperatures of 350 and 400 °C, where the surface is predominantly CuO, all other annealing settings lead to mixed Cu^{+1}/Cu^{+2} states at the electrode surface.

To further support the observations made from the Cu spectral features, the O $1s$ core level was measured for both samples with varying annealing temperature (figure 6(c)) and duration (figure 6(f)). The O $1s$ line shows a complex overall line shape with a number of contributing chemical state peaks. They are helpful in distinguishing clearly between features stemming from CuO and $Cu(OH)_2$. The observed differences with increasing annealing temperature agree well with those made from the Cu spectra, confirming the changes in Cu oxidation state and chemical environment. Samples annealed at 350 and 400 °C show a clear, intense peak from CuO. For samples annealed for varying duration at 250 °C a clear increase in hydroxide species with time is observed, in parallel to increases of the higher BE feature in the Cu $2p_{3/2}$ core level. As with the Cu core levels, the here observed O $1s$ BEs agree well with previously reported reference spectra [33–36].

3.3. Electrochemical performance
The annealed electrodes were electrochemically tested for their glucose sensing performance through chronoamperometric characterisation, by applying a measurement bias voltage of 0.25 V and recording the response current between the working and counter electrodes (see figures 5 and 6 in the supplementary information for all chronoamperometry response curves). Subsequently, the respective calibration curves versus the analyte were extracted from the steady-state current level for each glucose concentration (see figure 7). Interestingly, different CuO samples produced varying biosensor performance characteristics with substantially different limit of detection, linearity, and sensitivity. This is a clear indication as to how critical the exact morphology and composition of CuO is in any non-enzymatic electrochemical biosensor.

Figure 7. Glucose calibration curves for annealed electrodes at (a) varying temperatures at a constant time of 5 h, and (b) varying times at a constant temperature of 250 °C. The included error bars are derived from the standard deviation from three repetitive readings.

Two linear ranges were observed for each sensor, one for lower and one for higher concentrations. This is generally observed for electrochemical glucose biosensors [43]. The corresponding linear range values were extracted by linear fits of the respective calibration curve part that corresponded to a value of regression coefficient larger than 0.99. The limit of detection (LOD) was calculated as three times the standard deviation (SD) of the mean blank measurements i.e. pure 0.1 M NaOH without any glucose added. In this case, the standard deviation and error for each concentration was calculated from the last 10 s of the respective chronoamperometry measurement, as the current is observed to stabilise. The so extracted LODs are summarised in table 1.

The temperature dependent data show that the 150 °C sample is the best biosensor across the extracted figures of merit, e.g. showing the lowest LOD and highest saturation current. Whilst the surface chemistry is comparable between the samples annealed between 100 °C–200 °C showing mostly Cu^{+1}, the surface morphology evolves with an increasing overlayer formed on the polycrystalline Cu. The surface roughness from AFM is highest for the 150 °C sample, suggesting a strong influence of surface area on the sensing behaviour. The drop in performance at temperatures above 150 °C follows a strong decrease in surface roughness. Below 150 °C however, the surface roughness is indistinguishable from AFM, however subtle differences in chemical states are observed in XPS suggesting that in this regime surface chemistry may be the dominating factor determining sensing behaviour.

For the variation of annealing duration at 250 °C no distinct changes in surface roughness from AFM are observed and only small changes in morphology can be detected in SEM. In contrast a clear increase in hydroxyl groups on the electrode surface with annealing duration can be seen in the XPS data. This increase in

Table 1. Comparison of the sensing results for Cu electrodes after annealing in varying conditions, including the limit of detection (LOD) and the range Δ and slope (sensitivity) S of the two linear ranges. t_c refers to the calcination time and T_c refers to the calcination temperature.

t_c h	T_c °C	LOD μM	Δ_1 mM	S_1 $\mu A/mM$	Δ_2 mM	S_2 $\mu A/mM$
5	100	47	0.10–1.00	3.59	6–10	0.16
5	150	34	0.01–1.00	8.72	4–10	2.73
5	200	188	0.01–0.70	8.71	4–10	2.28
5	250	58	0.01–1.00	7.23	4–10	2.86
1	250	28	0.01–0.50	5.61	2–10	1.02
2	250	55	0.20–1.00	4.45	4–10	0.87
3	250	105	0.01–1.00	3.75	2–10	1.15
5	250	58	0.01–1.00	7.23	4–10	2.86
8	250	72	0.20–1.00	7.47	2–10	3.22
12	250	86	0.50–1.00	16.92	2–10	2.10
24	250	76	0.70–4.00	8.07	6–10	2.39

hydroxylation can increase the adsorption of glucose on the electrode surface consequently leading to the observed increase in current with concentration, particularly for the 8–24 h annealed samples as seen in figure 7(b). Such an increase in absorption energy of glucose and other saccharides with hydroxylation was previously observed for a number of inorganic surfaces [44–46].

Interference is another significant factor for glucose sensors as the electrochemical response can be affected by common interferents present in human blood or interstitial fluid, such as fructose, galactose, uric and ascorbic acid. The current responses for glucose and the interferents for all samples is included in table 1 in the supplementary information. In terms of sensor selectivity, the dependence of the sensor characteristics on CuO growth seems to be even more critical. Whilst all of the sensors exhibit increased selectivity to glucose, interference from common analytes (figure 8) dramatically decreases with increasing annealing temperature and interestingly, reducing the respective annealing time. Across all measurements the ascorbic acid shows the most significant interference amongst the different interfering species explored. At low temperatures the interference is large including for the 150 °C sample, which showed the best sensing performance in the chronoamperommetric experiments. At 200 and 250 °C very low levels of interference are observed (see figure 8(a)). The relative response to all interferents at 250 °C is comparable for annealing duration between 1 and 8 h. It only increases at longer annealing duration of 12 and 24 h. When both chronoamperommetric and interference results are combined, the sample annealed at 250 °C for 8 h is the best overall glucose sensor.

4. Conclusions

In this study non-enzymatic glucose sensors based on copper oxide are successfully prepared on flexible polyimide substrates necessary for future integration into PCB sensing platforms and for application in wearable sensors. The results clearly show the influence of both annealing temperature and duration on the physico-chemical surface characteristics and consequently the electrochemical sensing behaviour.

Whilst previous studies routinely characterise the surface morphology of such oxide-based biosensors, it alone cannot explain the differences observed here. It is clear that the final performance is dependant on a complex interaction of both the surface morphology as well as the surface chemistry. Different regimes across temperature and duration can be identified. Whilst in some regions changes in sensing performance can be directly correlated to surface roughness and morphology, other regions show clear influence of the surface chemistry of the as-prepared electrodes (e.g. across different annealing duration at a temperature of 150 °C). Overall, the data suggests that an anneal at 250 °C for 8 h provides the best compromise between sensor performance and low interference.

The presented results motivate further exploration of the underlying mechanisms resulting in the observed relationship between physico-chemical characteristics and sensing performance. In particular, the interference results warrant further exploration to understand the stark differences observed, including both experimental as well as theoretical approaches as applied in other application areas (e.g. saccharide absorption on varying copper surfaces). Furthermore, future studies need to include dynamic *in situ* characterisation of the solid/liquid interface during electrochemical experiments to gain an understanding of changes to the copper surface during operation.
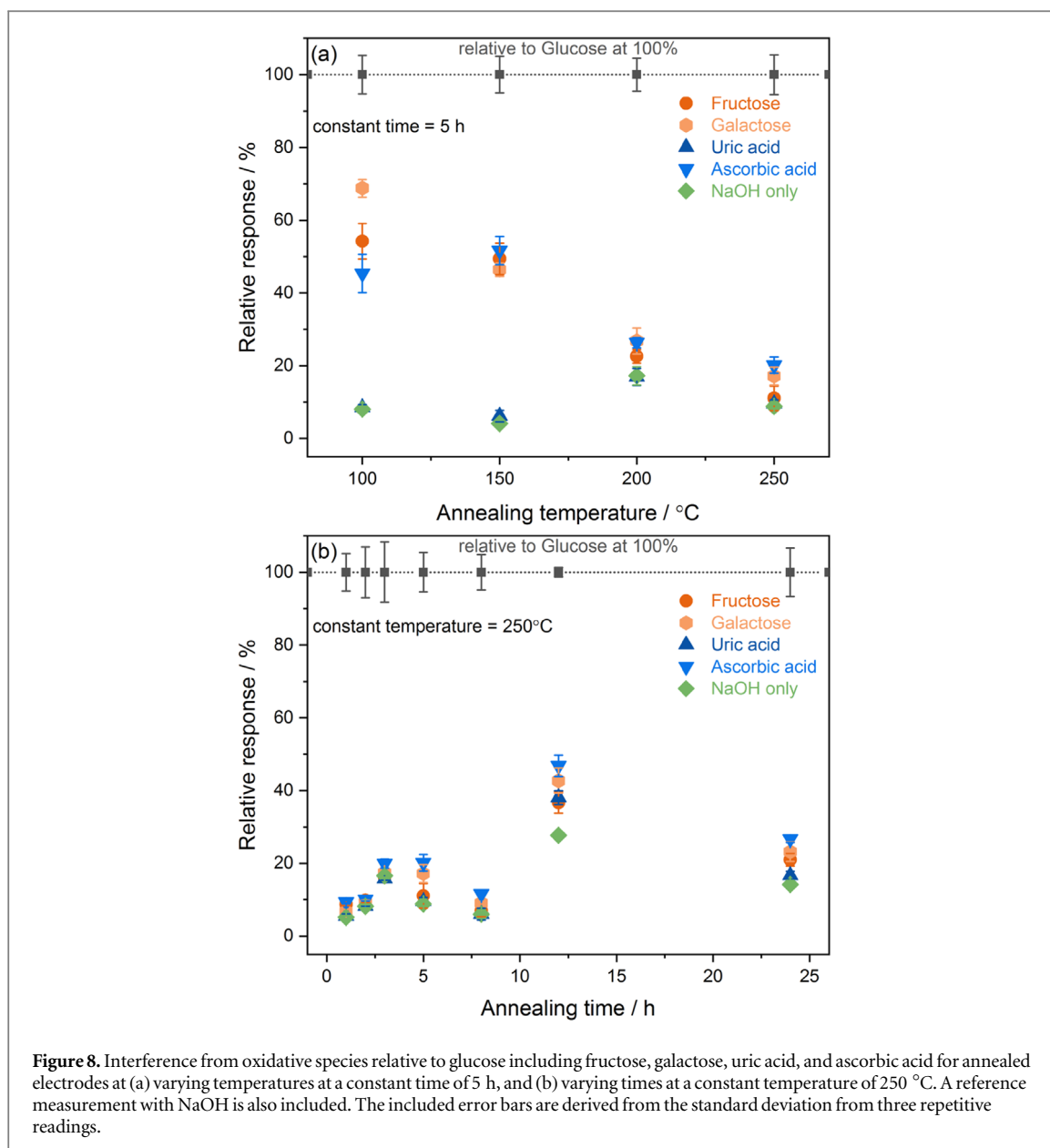
Figure 8. Interference from oxidative species relative to glucose including fructose, galactose, uric acid, and ascorbic acid for annealed electrodes at (a) varying temperatures at a constant time of 5 h, and (b) varying times at a constant temperature of 250 °C. A reference measurement with NaOH is also included. The included error bars are derived from the standard deviation from three repetitive readings.

Data availability statement

The data that support the findings of this study are available upon reasonable request from the authors.

ORCID iDs

Ayse Ay ⓘ https://orcid.org/0000-0002-1814-1616

Despina Moschou https://orcid.org/0000-0001-9175-5852

Anna Regoutz https://orcid.org/0000-0002-3747-3763

References

[1] Boyko E J *et al* (ed) 2021 *IDF Diabetes Atlas* X edn (International Diabetes Federation)

[2] Kondepati V R and Heise H M 2007 *Anal. Bioanal.Chem.* **388** 545–63

[3] Heller A and Feldman B 2008 *Chem. Rev.* **108** 2482–505

[4] Dhara K and Mahapatra D R 2018 *Microchim. Acta* **185** 49

[5] Hwang D W, Lee S, Seo M and Chung T D 2018 *Anal. Chim. Acta* **1033** 1–34

[6] Zhu H, Li L, Zhou W, Shao Z and Chen X 2016 *J. Mater. Chem. B* **4** 7333–49

[7] Wang G, He X, Wang L, Gu A, Huang Y, Fang B, Geng B and Zhang X 2013 *Microchim. Acta* **180** 161–86

[8] Bruen D, Delaney C, Florea L and Diamond D 2017 *Sensors* **17** 1866

[9] Chen J T, Zhang F, Wang J, Zhang G A, Miao B B, Fan X Y, Yan D and Yan P X 2008 *J. Alloys Compd.* **454** 268–73

[10] Nery E W, Kundys M, Jeleń P S and Jönsson-Niedziółka M 2016 *Anal. Chem.* **88** 11271–82

[11] Teymourian H, Barfidokht A and Wang J 2020 *Chem. Soc. Rev.* **49** 7671–709

[12] Oliver N S, Toumazou C, Cass A E G and Johnston D G 2009 *Diabetic Medicine* **26** 197–210

[13] Reitz E, Jia W, Gentile M, Wang Y and Lei Y 2008 *Electroanalysis* **20** 2482–6

[14] Li C, Yamahara H, Lee Y, Tabata H and Delaunay J J 2015 *Nanotechnology* **26** 305503

[15] Huang J, Zhu Y, Yang X, Chen W, Zhou Y and Li C 2015 *Nanoscale* **7** 559–69

[16] Medeiros N G, Ribas V C, Lavayen V and Da Silva J A 2016 *J. Solid State Electrochem.* **20** 2419–26

[17] Zhong Y, Shi T, Liu Z, Cheng S, Huang Y, Tao X, Liao G and Tang Z 2016 *Sensors and Actuators, B: Chemical* **236** 326–33

[18] Ashok A, Kumar A and Tarlochan F 2019 *Appl. Surf. Sci.* **481** 712–22

[19] Jagadeesan M S, Movlaee K, Krishnakumar T, Leonardi S G and Neri G 2019 *J. Electroanal. Chem.* **835** 161–8

[20] Vinoth V, Shergilin T D, Asiri A M, Wu J J and Anandan S 2018 *Mater. Sci. Semicond. Process.* **82** 31–8

[21] George J M, Antony A and Mathew B 2018 *Microchimica Acta* **185** 358

[22] Verma N and Kumar N 2019 *ACS Biomaterials Science and Engineering* **5** 1170–88

[23] Naikoo G A, Salim H, Hassan I U, Awan T, Arshad F, Pedram M Z, Ahmed W and Qurashi A 2021 *Frontiers in Chemistry* **9** 748957

[24] Aun T T, Salleh N M, Ali U F M and Manan N S A 2021 *Non-Enzymatic Glucose Sensors Involving Copper: an Electrochemical Perspective* 1–57

[25] Naikoo G A *et al* 2022 *Bioeng Transl Med.* **7** e10248

[26] Jiang L C and Zhang W D 2010 *Biosens. Bioelectron.* **25** 1402–7

[27] Luo S, Su F, Liu C, Li J, Liu R, Xiao Y, Li Y, Liu X and Cai Q 2011 *Talanta* **86** 157–63

[28] Liu G, Zheng B, Jiang Y, Cai Y, Du J, Yuan H and Xiao D 2012 *Talanta* **101** 24–31

[29] Li Y, Zhao M, Chen J, Fan S, Liang J, Ding L and Chen S 2016 *Sensors and Actuators, B: Chemical* **232** 750–7

[30] Li G and Wen D 2020 *J. Mater. Chem. B* **8** 3423–36

[31] Dupont (USA) 2020 DuPont^TM Kapton *Summary of Properties* vol EI-10142 (USA: Dupont)

[32] Yuan L, Wang Y, Mema R and Zhou G 2011 *Acta Mater.* **59** 2491–500

[33] Larson P E 1974 *J. Electron. Spectrosc. Relat. Phenom.* **4** 213–8

[34] Chawla S K, Sankarraman N and Payer J H 1992 *J. Electron. Spectrosc. Relat. Phenom.* **61** 1–18

[35] Ghijsen J, Tjeng L H, van Elp J, Eskes H, Westerink J, Sawatzky G A and Czyzyk M T 1988 *Phys. Rev. B* **38** 11322–30

[36] Tahir D and Tougaard S 2012 *Journal of Physics Condensed Matter* **24** 175002

[37] Panzner G, Egert B and Schmidt H P 1985 *Surf. Sci.* **151** 400–8

[38] Scrocco M 1979 *Chem. Phys. Lett.* **63** 52–6

[39] Pauly N, Tougaard S and Yubero F 2014 *Surf. Sci.* **620** 17–22

[40] Barman S R and Sarma D D 1992 *J. Phys. Condens. Matter* **4** 7607–16

[41] Poulston S, Parlett P M, Stone P and Bowker M 1996 *Surf. Interface Anal.* **24** 811–20

[42] Miller A C and Simmons G W 1993 *Surf. Sci. Spectra* **2** 55–60

[43] Malhotra S, Tang Y and Varshney P K 2019 *Chemical Papers* **73** 1987–96

[44] Liu Q, Laskowski J S, Li Y and Wang D 1994 *Int. J. Miner. Process.* **42** 251–66

[45] Laskowski J S, Liu Q and O'Connor C T 2007 *Int. J. Miner. Process.* **84** 59–68

[46] Lee S G, Choi J I, Koh W and Jang S S 2013 *Appl. Clay Sci.* **71** 73–81